

# Dynamical quantum typicality: A simple method for investigating transport properties applied to the Holstein model

Petar Mitrić\*

*Institute of Physics Belgrade, University of Belgrade, Pregrevica 118, 11080 Belgrade, Serbia*

We examine the practical applicability of the so-called dynamical quantum typicality (QT) for the calculation of the frequency dependent mobility in electron-phonon systems. The QT approach relies on the insight that even a single, randomly chosen pure state within a high-dimensional Hilbert space can effectively represent the entire statistical ensemble. This significantly simplifies the calculation of the current-current correlation function, which in turn, within the linear response theory, is directly related to the frequency dependent mobility. The time evolution operator  $e^{-iHt}$  and the Boltzmann factor  $e^{-\beta H}$  are handled using the Runge-Kutta scheme. As a result, we achieve a simple, transparent method that is easy to implement, with computer memory requirements and computational effort scaling linearly with the Hilbert space dimension and the time grid length. Although this approach is quite general, we restrict our numerical results to the Holstein model for which several reliable benchmarks are available. We demonstrate that the QT effectively complements other currently employed methods by overcoming some of their inherent limitations.

## I. INTRODUCTION

The study of charge carrier transport is fundamental for the advancement of both the theoretical understanding and practical applications, as it directly impacts the performance of electronic devices [1, 2]. Quantities such as frequency dependent mobility  $\mu(\omega)$  and time-dependent diffusion constant  $D(t)$  encode crucial information about transport behavior [3, 4]. In principle, these can be calculated using the linear response theory, à la Kubo, which relates them to the current-current correlation function  $C_{jj}(t)$  [5–7]. Yet, Kubo’s approach does not contain a concrete recipe for calculating  $C_{jj}(t)$ .

Over the years, numerous approximate methods for the calculation of transport properties have been developed, each with a specific purpose and varying degrees of success [8–11]. Some focus exclusively on the lowest-order Feynman diagram, i.e., the bubble term [12–17]—sometimes even with extremely high precision—but they neglect everything else, often without justification. Others approximately take into account the vertex corrections as well [18, 19], but face certain limitations: momentum average approximation [20], to the best of our knowledge, works only in the zero-temperature case; the analytic unitary transformation [21] has diverging DC mobility, requiring the ad hoc introduction of some scattering time  $\tau$ ; and the Boltzmann approach is applicable only in the weak coupling limit [22, 23], to name a few. Even if some highly accurate approximate method emerged, one would need to demonstrate its accuracy by benchmarking it against exact results, which highlights the persistent need for numerically exact methods.

Several notable numerically exact methods have been

developed [24–26], including the finite temperature Lanczos method (FTLM) [27–30], Chebyshev or kernel polynomial method (KPM) [31, 32], quantum Monte Carlo (QMC) [33–35], and hierarchical equations of motion (HEOM) [36, 37]. Each method, though exact in principle, has practical limitations. FTLM suffers from numerical instabilities, particularly the loss of orthogonality of the so-called Lanczos vectors at high expansion orders, which can be overcome but at the expense of significant computational resources. Additionally, FTLM requires substantial computer memory for storing some auxiliary states, restricting its applicability to small system sizes. KPM avoids the numerical instabilities of FTLM but shares its high memory requirements for auxiliary states, which makes reaching large system sizes also infeasible [32]. While memory-efficient versions of KPM exist, the computational cost scales quadratically with the expansion order, which is typically large, further limiting practicality. On the other hand, QMC is particularly appealing for its ability to examine significantly larger systems and produce reliable error estimates. However, it too faces challenges: the imaginary-time formulation struggles with numerically ill-defined analytic continuation [37, 38], while the real-time version is hindered by the sign problem [39], thus giving accurate results for  $C_{jj}(t)$  only for short propagation times [37]. HEOM overcomes many of these issues, enabling studies of large systems and long-time dynamics. Yet, it suffers from instabilities at strong couplings or low temperatures, while the application to general Hamiltonian can be difficult or impossible. Thus, no single method works universally across all regimes, necessitating a combination of approaches to achieve a reliable physical picture. The development of new methods remains crucial to addressing these gaps.

Calculating the current-current correlation function  $C_{jj}(t) = \text{Tr} [e^{-\beta H} e^{iHt} j e^{-iHt} j] / \text{Tr} [e^{-\beta H}]$  requires tackling two important questions: i) how to calculate

\* mitricp@ipb.ac.rs

the trace? ii) how to deal with the time evolution  $e^{-iHt}$  and the Boltzmann  $e^{-\beta H}$  factors? The challenge stems from the exponential growth of the Hilbert space with the system size; otherwise, exact diagonalization would easily solve both of these problems. This difficulty can be leveraged to our advantage, at least in addressing the first of these challenges, using the so-called stochastic trace estimation.

Originally introduced by Girard [40] and Hutchinson [41], stochastic trace estimation relies on an insight that the trace of an arbitrary operator can be approximated by first calculating its expectation value with respect to randomly chosen vectors and then averaging the obtained results over many (ideally infinite) such vectors [42–46]. However, the error obtained by using only a few such random vectors is often quite small in physically relevant problems, such as the one we are examining here. This is because the relative error typically decreases with the effective size of the Hilbert space [47]. The effective size is often so immense, that accurate results can be obtained using just a single random vector. This approach is known as (dynamical) quantum typicality (QT) [48–56].

The second challenge that we mentioned, concerning the factors  $e^{-iHt}$  and  $e^{-\beta H}$ , can be addressed using the well-known Runge-Kutta method [57, 58]. Although other techniques can also be used, this choice is particularly appealing due to the fact that it stores only a small number of auxiliary states, thereby enabling the study of larger systems within available computer memory resources.

In this work, we test the advantages and drawbacks of the described methodology by investigating the transport properties within one of the simplest electron-phonon models—the one-dimensional Holstein model [59, 60]. This model is particularly suitable for our study due to the availability of highly accurate benchmark results in the literature, obtained using the HEOM method [36, 37, 61], which allow for an in-depth comparison with the predictions of the QT approach across a wide range of parameter regimes.

The remainder of this paper is organized as follows: Section II A introduces the Holstein Hamiltonian. The key results from the linear response theory are briefly summarized in Sec. II B. The stochastic trace estimation, its practical implementation for computing the trace in  $C_{jj}(t)$ , and the Runge-Kutta scheme are reviewed in Secs. II C, II D, and II E, respectively. In Sec. III, we present and analyze the main QT numerical results, providing a detailed comparison with benchmarks from the literature. Concluding remarks, addressed in Sec. IV, discuss the advantages and drawbacks of QT compared to other exact methods, and discuss its potential applications to other models as well. Additional numerical results are included in the Supplemental Material (SM) [62].

## II. THEORETICAL CONSIDERATIONS

### A. Model

We examine the one-dimensional Holstein, on a lattice with  $N$  sites, with periodic boundary conditions. The corresponding Hamiltonian is given by

$$H = -t_0 \sum_{\langle i,j \rangle} (c_i^\dagger c_j + H.c.) - g \sum_i c_i^\dagger c_i (a_i^\dagger + a_i) + \omega_0 \sum_i a_i^\dagger a_i, \quad (1)$$

where  $c_i^\dagger$  and  $c_i$  ( $a_i^\dagger$  and  $a_i$ ) are electron (phonon) creation and annihilation operators,  $t_0$  is the hopping parameter,  $g$  is the electron-phonon coupling constant,  $\omega_0$  is the phonon frequency, while it is customary to also introduce the dimensionless strength of the electron-phonon interaction  $\lambda = g^2/(2\omega_0 t_0)$ . In the rest of this paper, we set the hopping parameter  $t_0$ , the Planck constant  $\hbar$ , and the Boltzmann constant  $k_B$  to 1.. Furthermore, we assume that there is only a single electron in the conduction band. This is a standard assumption, as this model should qualitatively describe weakly doped organic semiconductors.

Due to the possibly infinite number of phononic excitations, the Hilbert space is actually infinite-dimensional. To apply the QT method, Hilbert space needs to be truncated by limiting the total number of phonons in a system to be less or equal than some finite number  $M$ . Then, it is easy to show that the dimension of Hilbert space is given by

$$d = N \binom{N+M}{N}. \quad (2)$$

In all parameter regimes we examined, we tried to use sufficiently large  $N$ , so that the results would be representative of the thermodynamic limit  $N \rightarrow \infty$ . In addition, for a given  $N$ , the value for  $M$  was always chosen to be sufficiently large to ensure that the calculated quantities converged with respect to this parameter  $M$ ; see Sec. A of SM [62].

### B. Frequency-dependent mobility

The central quantity of this work is frequency dependent mobility  $\mu(\omega)$ , which is just the optical conductivity normalized to the concentration of charge carriers. Theoretically,  $\mu(\omega)$  is related to the current-current correlation function  $C_{jj}(t)$  within Kubo linear response theory [5, 6]

$$\mu(\omega) = \frac{2 \tanh\left(\frac{\beta\omega}{2}\right)}{\omega} \int_0^\infty \cos(\omega t) \text{Re} C_{jj}(t) dt. \quad (3)$$

While  $\text{Re } C_{jj}(t)$  contains all information about  $\mu(\omega)$ , it is sometimes [9, 37] more convenient to analyze an equivalent quantity: the time dependent diffusion constant, which describes the growth rate  $D(t) = \frac{1}{2} \frac{d}{dt} (\Delta x(t))^2$  of the charge carrier quantum-mechanical spread,  $\Delta x(t) = \sqrt{\langle (x(t) - x(0))^2 \rangle}$ . The diffusion constant is mathematically related to  $\text{Re } C_{jj}(t)$  via the following expression

$$D(t) = \int_0^t dt' \text{Re } C_{jj}(t'). \quad (4)$$

From Equations (3) and (4), it directly follows that  $\mu(\omega = 0) = D(t \rightarrow \infty)/T$ . This is the famous Einstein relation, which shows that for the DC mobility  $\mu(\omega = 0)$  to be finite, the time-dependent diffusion constant must saturate to a constant value at large times.

Before explaining how we calculate  $C_{jj}(t)$  in practice, let us first emphasize that  $\mu(\omega)$  satisfies the so-called optical sum rule, which in the case of the Holstein model in the thermodynamic limit ( $N \rightarrow \infty$ ) reads as follows

$$\int_0^\infty d\omega \mu(\omega) = -\frac{\pi}{2} \langle H_{\text{el}} \rangle. \quad (5)$$

Here,  $\langle H_{\text{el}} \rangle$  is the expectation value of the electronic part of the Hamiltonian, which is given by the first line of Eq. (1). Since the method we will be using can be applied only on systems with finite number of lattice sites, the extent to which Eq. (5) is satisfied, expressed using the relative error

$$\delta = \frac{|\int_0^\infty d\omega \mu(\omega) + \frac{\pi}{2} \langle H_{\text{el}} \rangle|}{-\frac{\pi}{2} \langle H_{\text{el}} \rangle}, \quad (6)$$

can serve as an indicator of the presence of finite-size effects. This is because the dynamical transport properties (i.e., the left-hand side of Eq. (5)) typically converge slower with respect to  $N$ , than static quantities (i.e., the right-hand side of Eq. (5)).

All of this motivates why our theoretical work boils down to the calculation of both  $C_{jj}(t)$  and  $\langle H_{\text{el}} \rangle$ . This will be discussed in subsequent subsections.

### C. Stochastic trace estimation

The quantities  $C_{jj}(t) = \langle j(t)j \rangle$  and  $\langle H_{\text{el}} \rangle$  are both of form  $\langle A \rangle = \text{Tr} [e^{-\beta H} A] / \text{Tr} [e^{-\beta H}]$ , for an appropriate choice of  $A$ . A key step in their calculation is evaluating the traces of various operators, collectively denoted as  $X$  (e.g.,  $X = e^{-\beta H} A$ ,  $X = e^{-\beta H}$ ). At first glance, calculating traces seems straightforward, as it requires summing the diagonal elements of  $X$  in an arbitrary basis. However, in our case, this task becomes computationally challenging due to the large Hilbert space and

the complexity of  $X$ , as it typically involves products of other operators, some of which are exponentials of additional operators. One of the ways to overcome this challenge is to introduce mutually independent complex random variables  $c_i$  with zero mean and variance equal to  $E [|c|^2]$ . Then, the trace of arbitrary  $X$  can be rewritten as follows

$$\begin{aligned} \text{Tr } X &= \sum_{i,j} \delta_{i,j} \langle i | X | j \rangle = \sum_{i,j} \frac{E [c_i^* c_j]}{E [|c|^2]} \langle i | X | j \rangle \\ &= \frac{1}{E [|c|^2]} E \left[ \left( \sum_i c_i^* \langle i | \right) X \left( \sum_j c_j | j \rangle \right) \right] \\ &= \frac{E [\langle \psi | X | \psi \rangle]}{E [|c|^2]}, \end{aligned} \quad (7)$$

where  $|i\rangle$  are (arbitrary chosen) basis vectors, while  $|\psi\rangle = \sum_i c_i |i\rangle$  can be interpreted as a randomly chosen vector from the Hilbert space. Equation (7) is an exact identity, known as the stochastic trace estimation [40–46], and in the case of large-dimensional systems generally requires much less computational effort than a straightforward approach for the evaluation of the trace.

By combining the stochastic trace estimation with the cyclic property of the trace  $\text{Tr} [e^{-\beta H} A] = \text{Tr} [e^{-\beta H/2} A e^{-\beta H/2}]$ , we see that the expectation value of arbitrary quantity  $A$  in the canonical ensemble can be expressed as

$$\langle A \rangle = \frac{E [\langle \psi | e^{-\beta H/2} A e^{-\beta H/2} | \psi \rangle]}{E [\langle \psi | e^{-\beta H} | \psi \rangle]} = \frac{E [\langle \psi_\beta | A | \psi_\beta \rangle]}{E [\langle \psi_\beta | \psi_\beta \rangle]}, \quad (8)$$

where  $|\psi_\beta\rangle = e^{-\beta H/2} |\psi\rangle$ . When calculating the expectation values  $E[\cdot]$ , the number of random vector realizations, required for accurate results, is oftentimes actually quite small. The relative error one would obtain in Eq. (8) by using only  $R$  random vectors scales as  $\mathcal{O}(1/\sqrt{R d_{\text{eff}}})$ , where  $d_{\text{eff}} = \text{Tr} [e^{-\beta(H-E_0)}]$  is the effective dimension of the Hilbert space, and  $E_0$  is the ground state energy. Consequently, in cases where the effective Hilbert space is large, as it typically is in this work, a single random vector suffices for Eq. (8). This approach is known as (dynamical) quantum typicality (QT) [48, 49].

Another factor that can affect the relative error in the QT approach is the selection of the probability distribution for the random coefficients  $c_i$ . As discussed in Refs. [32, 49], various distributions are commonly used, each with its own advantages, but determining the optimal distribution *a priori* remains challenging. In this work, we will employ the Gaussian probability distribution with zero mean for  $c_i$ , as it has the property that the relative error is independent of the choice of the basis  $|i\rangle$ . The variance of this distribution can be chosen arbitrarily, as Eq. (8) does not depend on  $E [|c|^2]$ .

#### D. Quantum typicality approach for computing current-current correlation functions

Let us now demonstrate how the QT approach, which we summarized in the previous subsection, can be applied for the calculation of the current-current correlation function  $C_{jj}(t) = \langle j(t)j \rangle$ . Starting from Eq. (8) with only a single random vector  $|\psi\rangle$ , and setting  $A = j(t)j = e^{iHt} j e^{-iHt} j$ , we obtain

$$\begin{aligned} C_{jj}(t) &\approx \frac{\langle \psi | e^{-\beta H/2} e^{iHt} j e^{-iHt} j e^{-\beta H/2} | \psi \rangle}{\langle \psi | e^{-\beta H} | \psi \rangle} \\ &= \frac{\langle \psi_\beta(t) | j | \phi_\beta(t) \rangle}{\langle \psi_\beta(t) | \psi_\beta(t) \rangle}, \end{aligned} \quad (9)$$

where we defined

$$|\psi_\beta(t)\rangle = e^{-iHt} e^{-\beta H/2} |\psi\rangle, \quad (10)$$

$$|\phi_\beta(t)\rangle = e^{-iHt} j e^{-\beta H/2} |\psi\rangle. \quad (11)$$

The current operator  $j$  is determined as the time derivative of the polarization operator  $P = \sum_j j c_j^\dagger c_j$ , and in the Holstein model assumes the following form

$$j = \frac{\partial P}{\partial t} = -i[P, H] = it_0 \sum_r \left( c_{r+1}^\dagger c_r - c_r^\dagger c_{r+1} \right). \quad (12)$$

A completely analogous approach can also be applied to calculate  $\langle H_{el} \rangle$ , which is even simpler since it is a static quantity and does not involve time evolution. In fact, both  $C_{jj}(t)$  and  $\langle H_{el} \rangle$  (as well as some additional quantities as well) can all be calculated simultaneously using QT, as they can all share the same random vectors  $|\psi\rangle$ .

In order to perform all of these calculations, we first need to find a way to deal with time evolution  $e^{-iHt}$  and Boltzmann  $e^{-\beta H}$  factors in Eqs. (10) and (11). This is what we discuss next.

#### E. Runge-Kutta scheme

Several approaches have been proposed [27–32, 57, 58] for handling the exponentials  $e^{-iHt}$  and  $e^{-\beta H}$  in Eqs. (10) and (11). However, we have chosen the Runge-Kutta scheme [57, 58] due to its ability to minimize the need for storing excessive auxiliary states in computer memory. This choice allows us to handle larger system sizes within the available memory, which in turn increases the effective dimension of the Hilbert space, further justifying the use of the QT approach. In the remainder of this section, we briefly review the Runge-Kutta scheme for a time-independent Hamiltonian. We demonstrate its application for  $e^{-iHt}$ , while the treatment of  $e^{-\beta H}$  follows analogously.

To evolve a wave function  $|\psi\rangle$ , we first break the total evolution into small time steps  $dt$  as follows

$$|\psi(t)\rangle = e^{-iHt} |\psi\rangle = \underbrace{e^{-iHdt} e^{-iHdt} \dots e^{-iHdt}}_{N_t \text{ times, such that } N_t dt = t} |\psi\rangle. \quad (13)$$

Then, the evolution over each  $dt$  can be straightforwardly accomplished, by expanding the time evolution operator  $e^{-iHdt}$  in the Taylor series up to some order  $n$

$$|\psi(dt)\rangle \equiv e^{-iHdt} |\psi\rangle \approx \sum_{l=0}^n \frac{(-iHdt)^l}{l!} |\psi\rangle. \quad (14)$$

To explain how Eq. (14) is implemented in practice, let us introduce

$$|f_j\rangle = \sum_{l=0}^{n-j} \frac{j!}{(j+l)!} (-iHdt)^l |\psi\rangle, \quad (15)$$

which evidently satisfy the following recurrence relations

$$|f_{j-1}\rangle = |\psi\rangle + \frac{(-iHdt)}{j} |f_j\rangle. \quad (16)$$

From Eqs. (15) and (16) we can see that  $|f_n\rangle = |\psi\rangle$  and  $|f_0\rangle = |\psi(dt)\rangle$ . Therefore, the expression in Eq. (14) can be evaluated using an iterative procedure. We begin with  $|f_n\rangle = |\psi\rangle$ , and apply Eq. (16) to calculate  $|f_j\rangle$  for  $j = n-1, n-2, \dots, 0$ , until  $|\psi(dt)\rangle = |f_0\rangle$  is obtained. It is important to note that the Runge-Kutta scheme does not necessarily preserve the normalization of the wave function. To address this, we manually adjust the wave function at each time step  $dt$  by multiplying  $|\psi(dt)\rangle$  by a real constant, ensuring that  $\langle \psi | \psi \rangle = \langle \psi(t) | \psi(t) \rangle$ .

Let us note that although the method used in this paper combines stochastic trace estimation with a single random vector, and the Runge-Kutta scheme for wave function propagation, we will refer to this entire approach as quantum typicality (QT) for brevity.

### III. RESULTS

In this section, we present and analyze the QT results for the current-current correlation function  $C_{jj}(t)$ , the frequency-dependent mobility  $\mu(\omega)$ , and the time-dependent diffusion constant  $D(t)$  across a wide range of parameter regimes, comparing them with HEOM and other benchmarks. Additionally, for each regime, we also report the relative accuracy  $\delta$  with which the optical sum rule is satisfied within QT.

In the weak coupling regime, electron-phonon scattering is also weak, meaning the electron must travel long distances to lose memory of its initial state. As a result, large number of lattice sites  $N$  are necessary

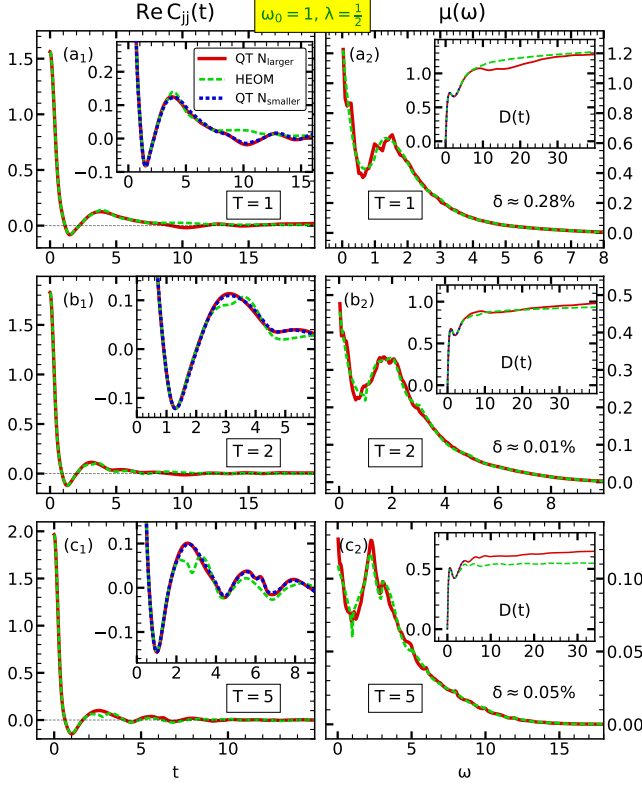


FIG. 1. Comparison of (a<sub>1</sub>)–(c<sub>1</sub>)  $\text{Re } C_{jj}(t)$  and (a<sub>2</sub>)–(c<sub>2</sub>)  $\mu(\omega)$  in the weak-intermediate coupling regime  $\omega_0 = 1$ ,  $\lambda = 1/2$  at  $T = 1, 2, 5$ . Insets of (a<sub>1</sub>)–(c<sub>1</sub>) show zoomed-in portions of the panels and additional QT results on smaller lattices. Panels (a<sub>2</sub>)–(c<sub>2</sub>) display the relative accuracy  $\delta$  of the optical sum rule within QT, with insets showing  $D(t)$ . The number of phonons  $M$  and lattice sites  $N$  used are: (a<sub>1</sub>)–(a<sub>2</sub>)  $(M, N)_{\text{larger}}^{\text{QT}} = (20, 11)$ ,  $(M, N)_{\text{smaller}}^{\text{QT}} = (19, 10)$ ,  $N^{\text{HEOM}} = 13$ ; (b<sub>1</sub>)–(b<sub>2</sub>)  $(M, N)_{\text{larger}}^{\text{QT}} = (34, 8)$ ,  $(M, N)_{\text{smaller}}^{\text{QT}} = (34, 7)$ ,  $N^{\text{HEOM}} = 10$ ; (c<sub>1</sub>)–(c<sub>2</sub>)  $(M, N)_{\text{larger}}^{\text{QT}} = (70, 6)$ ,  $(M, N)_{\text{smaller}}^{\text{QT}} = (60, 5)$ ,  $N^{\text{HEOM}} = 7$ .

to obtain results representative of the thermodynamic limit ( $N \rightarrow \infty$ ). At low temperatures, even larger values of  $N$  are needed. However, even if we consider only a single phonon per lattice site  $M = N$ , the dimension of the Hilbert space (as shown in Eq. (2)) scales as  $d \sim 4^N \sqrt{N/\pi}$ , which becomes an enormously large number for required  $N$ , which can involve several dozen lattice sites. This is why QT, in its present form, is not suitable for weak couplings and low temperatures, and the reason why we focus on intermediate and strong couplings with moderate and high temperatures.

The results for weak-intermediate coupling regime ( $\lambda = 1/2$ ), moderate temperature  $T = 1$  and phonon frequency  $\omega_0 = 1$  are presented in Figs. 1(a<sub>1</sub>) and 1(a<sub>2</sub>). In Fig. 1(a<sub>1</sub>) we observe an excellent agreement between methods. A small discrepancy in the current-current correlation function  $C_{jj}(t)$  between QT and HEOM is

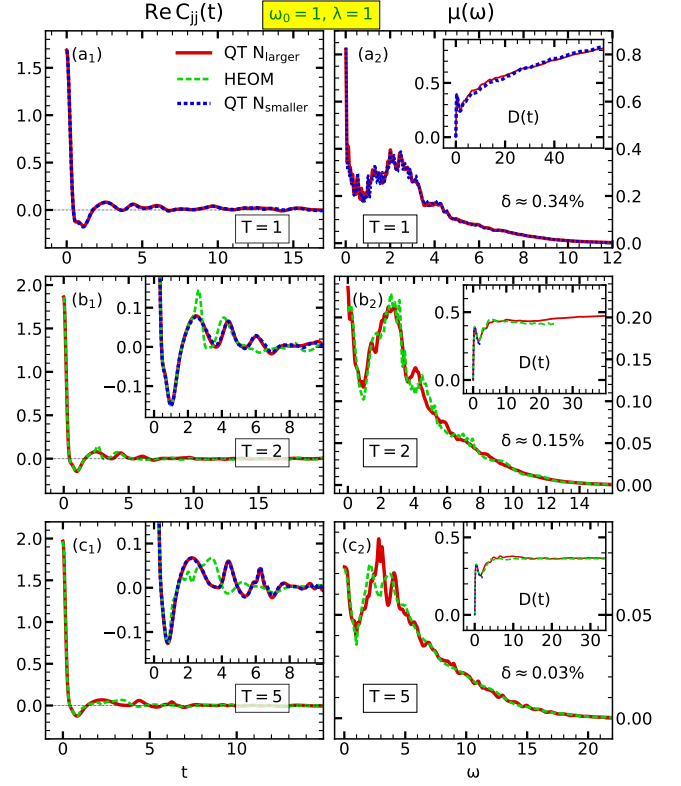


FIG. 2. Comparison of (a<sub>1</sub>)–(c<sub>1</sub>)  $\text{Re } C_{jj}(t)$  and (a<sub>2</sub>)–(c<sub>2</sub>)  $\mu(\omega)$  in the intermediate coupling regime  $\omega_0 = 1$ ,  $\lambda = 1$  at  $T = 1, 2, 5$ . Insets of (a<sub>1</sub>)–(c<sub>1</sub>) show zoomed-in portions of the panels and additional QT results on smaller lattices. Panels (a<sub>2</sub>)–(c<sub>2</sub>) display the relative accuracy  $\delta$  of the optical sum rule within QT, with insets showing  $D(t)$ . The number of phonons  $M$  and lattice sites  $N$  used are: (a<sub>1</sub>)–(a<sub>2</sub>)  $(M, N)_{\text{larger}}^{\text{QT}} = (21, 10)$ ,  $(M, N)_{\text{smaller}}^{\text{QT}} = (20, 9)$ ; (b<sub>1</sub>)–(b<sub>2</sub>)  $(M, N)_{\text{larger}}^{\text{QT}} = (33, 7)$ ,  $(M, N)_{\text{smaller}}^{\text{QT}} = (30, 6)$ ,  $N^{\text{HEOM}} = 10$ ; (c<sub>1</sub>)–(c<sub>2</sub>)  $(M, N)_{\text{larger}}^{\text{QT}} = (70, 6)$ ,  $(M, N)_{\text{smaller}}^{\text{QT}} = (60, 5)$ ,  $N^{\text{HEOM}} = 7$ .

visible only for  $t \sim 10$ . This is not a consequence of small finite size effects, even though HEOM results were obtained on a lattice with  $N_{\text{HEOM}} = 13$  sites, while QT method used  $N_{\text{larger}}^{\text{QT}} = 11$ . This can be concluded from the inset of Fig. 1(a<sub>1</sub>), where we demonstrate that the valley around  $t \sim 10$  actually converged with respect to the number of lattice sites  $N$ . Additional support for this statement is the fact that the relative accuracy  $\delta$  with which the optical sum rule is satisfied is good  $\delta \approx 0.276\%$ . It is worth noting that, in the QT method, for every parameter regime we always checked the convergence with respect to the total number of phonons  $M$ , which is actually quite easy to do, as explained in Sec. A of SM [62]. This analysis, together with the simplicity and transparency of the QT method, give us confidence that QT is indeed more accurate in this case. In contrast to QT, the HEOM method, although very

powerful, involves more complex numerical settings and is less straightforward, making it harder to determine whether small numerical inaccuracies have been fully eliminated [36, 37]. Despite all of this, we find that the agreement in frequency dependent mobility  $\mu(\omega)$  is excellent; see Fig 1(a<sub>2</sub>).

As the temperature increases, the discrepancies between QT and HEOM grow progressively more pronounced, becoming evident even at intermediate timescales; see Figs. 1(b<sub>1</sub>)–1(c<sub>1</sub>). At  $T = 5$ , a clear difference in  $C_{jj}(t)$ , between QT and HEOM can be seen in an inset, showing a closer view of Panel 1(c1). As in Fig. 1(a<sub>1</sub>), we checked that these differences are not due to the finite-size effects, and that QT also converged with respect to the total number of phonons. Present analysis, in combination with the discussion associated with Fig. 5 of Ref. [36], indicates that HEOM results are probably not fully converged with respect to the so-called maximum hierarchy depth [36, 37]. All of these factors reinforce our confidence in QT being more reliable than HEOM at higher temperatures, although the mismatch between the methods is not very large.

The general agreement between the QT and HEOM current-current correlation function, translates to a very good agreement between the frequency-dependent mobilities computed by these approaches; see Figs. 1(a<sub>2</sub>)–1(c<sub>2</sub>). Although this confirms that QT can actually provide accurate  $\mu(\omega)$ , it should be noted that the quantitative value of the DC mobility (and  $\mu(\omega)$  for very small  $\omega$ ) has somewhat larger error. This is because, for the time scales over which we propagate  $C_{jj}(t)$ , a clear plateau in the time-dependent diffusion constant  $D(t)$  does not always emerge. While longer time propagation is possible, it becomes computationally expensive. Nevertheless,  $\mu(\omega)$  should remain fairly accurate for frequencies that are not extremely small.

Current-current correlation functions and optical conductivities for intermediate coupling regime  $\lambda = 1$  are shown in Fig. 2. For higher temperatures  $T = 2, 3$ , we see again that QT is very reliable and more accurate than HEOM, as everything is completely analogous to the  $\lambda = 1/2$  case, while  $T = 1$  cannot be analyzed in a similar manner due to the unavailability of the HEOM result. At first glance, the QT numerical result for  $T = 1$  exhibits no apparent issues: the optical sum rule is satisfied with a high degree of accuracy  $\delta \approx 0.34\%$ , the thermodynamic limit seems to be reached, and (as shown in Sec. A of SM [62]) the results are fully converged with respect to the total number of phonons  $M$ . However, although the time-dependent diffusion constant  $D(t)$  is calculated over a substantial time range, it does not exhibit any signs of saturation; see the inset of Fig. 2(a<sub>2</sub>). We checked that this peculiarity persists even if we vary the lattice size, the number of phononic excitations, and the time step in the Runge-Kutta scheme; see Sec. B of SM [62]. Hence,

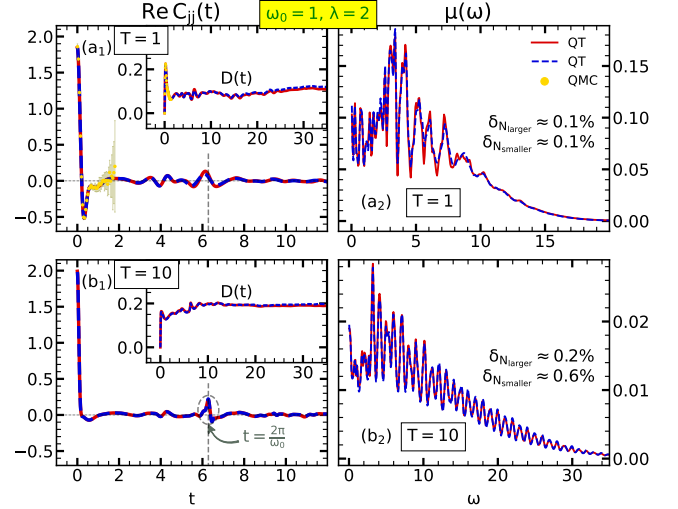


FIG. 3. Comparison of (a<sub>1</sub>)–(b<sub>1</sub>)  $C_{jj}(t)$  and (a<sub>2</sub>)–(b<sub>2</sub>)  $\mu(\omega)$  in the strong coupling regime  $\omega_0 = 1$ ,  $\lambda = 2$ , at  $T = 1, 10$ . The QMC results and the corresponding statistical error bars, shown only for  $T = 1$ , are reproduced from Fig. 6. of Ref. [37]. The QT predictions are shown for two different lattice sizes, denoted by  $N_{\text{larger}}$  and  $N_{\text{smaller}}$ . Insets of (a<sub>1</sub>)–(b<sub>1</sub>) show  $D(t)$ , while the relative accuracy  $\delta$  of the optical sum rule within QT is displayed in Panels (a<sub>2</sub>)–(c<sub>2</sub>). The number of phonons and lattice sizes used are: (a<sub>1</sub>)–(a<sub>2</sub>)  $(M, N)_{\text{larger}}^{\text{QT}} = (23, 10)$ ,  $(M, N)_{\text{smaller}}^{\text{QT}} = (20, 9)$ , and  $N^{\text{QMC}} = 10$  (b<sub>1</sub>)–(b<sub>2</sub>)  $(M, N)_{\text{larger}}^{\text{QT}} = (125, 5)$ ,  $(M, N)_{\text{smaller}}^{\text{QT}} = (130, 4)$ .

we can only conclude that the numerical results for the narrow peak  $|\omega| \lesssim 0.15$  are unreliable in Fig. 2(a<sub>2</sub>). Nevertheless,  $\mu(\omega)$  for larger  $\omega$  should be quite accurate; see Sec. B of SM [62].

Transport properties for strong interaction  $\lambda = 2$  are examined in Fig. 3. QT is actually most easily applied for large interaction strengths. This arises from the scaling of the Hilbert space with respect to  $N$  and  $M$  (see Eq. (2)), as well as the observation that such regimes, while requiring a large number of phonons, do not necessarily demand an extensive number of lattice sites to approximate the thermodynamic limit effectively. This is demonstrated in Fig. 3 by showing both that the optical sum rule is satisfied to a high degree of accuracy, and also by explicitly comparing QT results for two consecutive lattice sizes. Unfortunately, HEOM method cannot be applied here due to the fact that it cannot converge with respect to the maximum hierarchy depth. The only other independent benchmark that we use is the QMC, and we see that it is in excellent agreement with QT. Unfortunately, QMC is reliable only for relatively short times, until the sign problems starts showing up. Nevertheless, certain indirect indicators suggest that the QT results remain accurate even at longer times. These include rather fast attenuation of  $C_{jj}$ , as well as the appearance of a bump at  $t = 2\pi/\omega_0$  which is characteristic feature of such regimes [33, 37]. In Sec. C of SM [62], we also show the QT results for  $T = 2$  and  $T = 5$ .

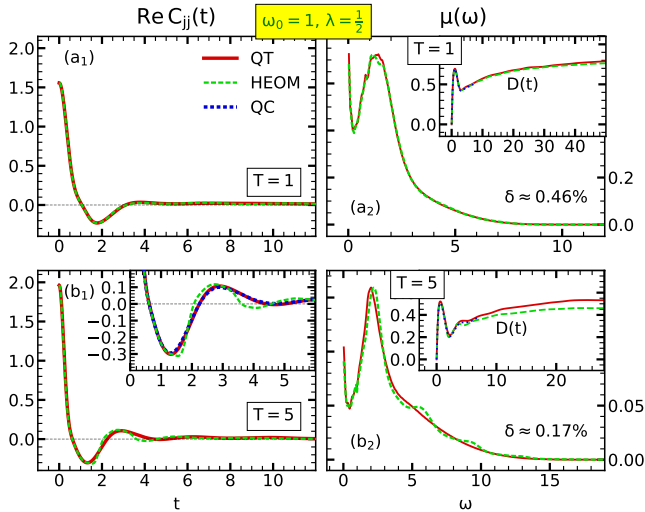


FIG. 4. Comparison of (a<sub>1</sub>)–(b<sub>1</sub>)  $C_{jj}(t)$  and (a<sub>2</sub>)–(b<sub>2</sub>)  $\mu(\omega)$  in the weak-intermediate coupling regime  $\omega_0 = 1/3$ ,  $\lambda = 1/2$ , at  $T = 1, 5$ . Panels (a<sub>2</sub>)–(b<sub>2</sub>) also show the relative accuracy  $\delta$  with which the optical sum rule is satisfied within QT, as well as the time-dependent diffusion constant  $D(t)$  in the insets. Inset of (b<sub>1</sub>) displays zoomed-in portion of the corresponding Panel, along with the results from quantum-classical (QC) method. The total number of phonons  $M$  and lattice sizes  $N$  used are: (a<sub>1</sub>)–(a<sub>2</sub>)  $M^{\text{QT}} = 45$ ,  $N^{\text{QT}} = 7$ , and  $N^{\text{HEOM}} = 10$ ; (b<sub>1</sub>)–(b<sub>2</sub>)  $M^{\text{QT}} = 130$ ,  $N^{\text{QT}} = 5$ ,  $N^{\text{HEOM}} = 6$ , and  $N^{\text{QC}} = 100$ .

Near the adiabatic limit ( $\omega_0 = 1/3$ ), the results for the weak-intermediate ( $\lambda = 1/2$ ), intermediate ( $\lambda = 1$ ), and strong coupling regime ( $\lambda = 2$ ) are presented in Figs. 4 and 5. The results are analogous to those we already obtained for  $\omega_0 = 1$ : we see that QT and HEOM current-current correlation functions are in excellent agreement for  $\lambda = 1/2$ ,  $T = 1$ , while at  $T = 5$  slight discrepancies arise already at intermediate timescales, but do not result in significant differences in  $\mu(\omega)$  (see Fig. 4(b<sub>2</sub>)). At intermediate and strong coupling regimes, QT demonstrates significantly better saturation of the diffusion constant  $D(t)$  at long times, closely mirroring the behavior observed in the  $\omega_0 = 1$  case. For  $\lambda = 1$ , QT and HEOM results agree well (see Fig. 5), but for  $\lambda = 2$  HEOM fails to converge with respect to the maximum hierarchy depth. Instead, QT is compared with the QMC benchmark. The agreement is excellent, although the QMC sign problem limits the verification of QT results to only short times.

Before moving on to the concluding Section, let us further examine the discrepancy between QT and HEOM results observed at  $\omega_0 = 1/3$ ,  $\lambda = 1/2$ ,  $T = 5$ . QT does not contain any inherent numerical instabilities in this case, and the only potential inaccuracies could emerge if the method did not fully converge with respect to both of its numerical parameters ( $N$  and  $M$ ). Convergence with respect to the total number of phonons

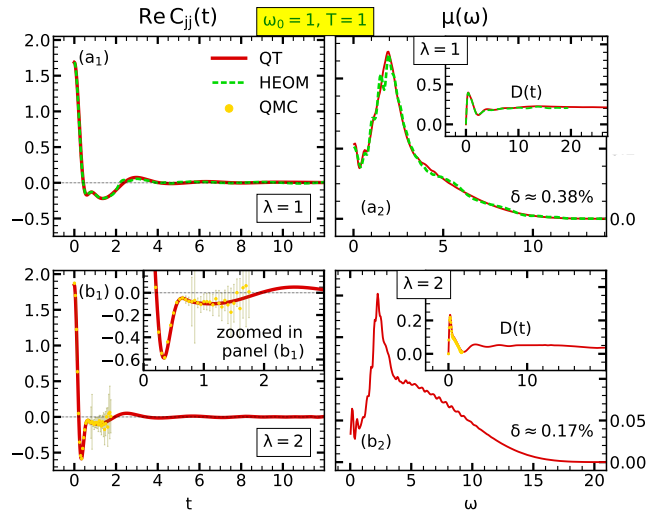


FIG. 5. Comparison of (a<sub>1</sub>)–(b<sub>1</sub>)  $C_{jj}(t)$  and (a<sub>2</sub>)–(b<sub>2</sub>)  $\mu(\omega)$  at  $T = 1$  in the intermediate  $\lambda = 1$  and strong coupling  $\lambda = 2$  regimes for  $\omega_0 = 1/3$ . Panels (a<sub>2</sub>)–(b<sub>2</sub>) also show the relative accuracy  $\delta$  with which the optical sum rule is satisfied within QT, as well as the time-dependent diffusion constant  $D(t)$  in the insets. The QMC data, shown with the corresponding statistical error bars, were reproduced from Fig. 10. of Ref. [37]. The total number of phonons  $M$  and lattice sizes  $N$  used are: (a<sub>1</sub>)–(a<sub>2</sub>)  $M^{\text{QT}} = 48$ ,  $N^{\text{QT}} = 7$ , and  $N^{\text{HEOM}} = 7$ ; (b<sub>1</sub>)–(b<sub>2</sub>)  $M^{\text{QT}} = 48$ ,  $N^{\text{QT}} = 7$ , and  $N^{\text{QMC}} = 7$ .

$M$  is straightforward, and has been performed as explained in Sec. A of SM [62]. However, verifying convergence with respect to the number of lattice sites  $N$  is more challenging. In the  $\omega_0 = 1$  case, we simply repeated QT calculation for two consecutive values of  $N$  and showed they coincided. This approach is much more difficult to perform in the regime we examine in Fig. 4(b<sub>1</sub>). It turns out that the lattice that we use  $N^{\text{QT}} = 5$  is just large enough to be considered in the thermodynamic limit. Any smaller lattices ( $N^{\text{QT}} \leq 4$ ) would suffer from finite-size effects (and would thus not coincide with the result for  $N^{\text{QT}} = 5$ ), while using larger lattice sizes would require substantial computational resources (we need  $M^{\text{QT}}/N^{\text{QT}} = 26$  phonons per lattice site). Although the optical sum rule is satisfied with high precision ( $\delta \approx 0.17\%$ ), suggesting that  $N^{\text{QT}} = 5$  is large enough to approximate the thermodynamic limit, this alone does not provide enough evidence to conclusively demonstrate that QT is more accurate than HEOM at intermediate timescales, where discrepancies between the methods arise. This can, however, be confirmed by exploiting the fact that  $\omega_0 = 1/3$  is relatively close to the adiabatic limit, while  $T = 5$  is quite high temperature. Hence, it is justified to use a quantum-classical approach, treating ions using Ehrenfest equations, while preserving a fully quantum description of the electron (see Ref. [63] for more details). In addition

to being simpler and numerically cheaper, the advantage of this method is the fact that we can apply it on systems with very large number of lattice sites, representative of the thermodynamic limit (in this case we use  $N = 100$ ). The obtained results are shown in the inset in Fig. 4(b<sub>1</sub>), where we see a complete agreement with QT. Hence, QT is indeed more accurate than HEOM in this regime.

#### IV. CONCLUSIONS AND OUTLOOK

In summary, we analyzed the application of stochastic trace estimation, using a single random vector, combined with the Runge-Kutta method (collectively referred to as QT), for calculating the transport properties in a simple electron-phonon model. Unlike the QMC, which is limited by the sign problem, we demonstrated that QT approach can compute current-current correlation functions up to significantly longer times, sufficient for determining frequency-dependent mobility via Kubo's linear response theory. Compared to HEOM, the QT can handle much stronger electron-phonon couplings. Even at intermediate couplings and higher temperatures, QT proved to be more accurate. Therefore, QT effectively addresses many of the limitations of QMC and HEOM. However, it should be noted that QT does not replicate all of their advantages: in particular, it cannot reach systems as large as QMC and HEOM. This is crucial for weak coupling and low temperature regimes, where a large number of lattices sites are necessary to reach the thermodynamic limit.

It is important to note that the stochastic trace estimation, used in QT, is also an integral part of FTLM [29] and KPM [32] as well. However, there are important differences. The main distinction stems from the way each of those methods handles the time evolution  $e^{-iHt}$  and Boltzmann  $e^{-\beta H}$  factors. In addressing these factors, both FTLM and KPM typically require storing a substantial number of auxiliary states. As a result, they tend to be quite memory-intensive, especially for problems involving high-dimensional Hilbert spaces, such as the one we examined in our study. In contrast, the Runge-Kutta approach, used in QT, only stores a few auxiliary states, allowing it to handle somewhat larger systems within the available computer memory. Furthermore, in larger systems, the effective dimension of

the Hilbert space is greater, allowing QT to achieve high accuracy even though it uses just a single random vector in the stochastic trace approximation. It is worth noting that KPM can also be adapted to store fewer auxiliary states, but this comes at a significantly higher computational cost [32]. Hence, as with HEOM and QMC, we find that QT overcomes some limitations of FTLM and KPM, but it does not retain all of their advantages. Specifically, propagating correlation functions to longer times is easier with FTLM and KPM. Nevertheless, this limitation is not crucial in the regimes where QT is most effective—namely, at intermediate and strong couplings—since, in these cases, the correlation function typically decays within a relatively short time interval.

Although our treatment in this work focused on the Holstein model, the same procedure can be readily applied to more general systems. The only adjustment required would be how the Hamiltonian  $H$  and the current operator  $j$  act on an arbitrary vector from the corresponding Hilbert space. However, it is important to be aware of some practical limitations of the QT approach. Specifically, our algorithm involves numerous matrix-vector multiplications, with the matrix typically being  $H$  or  $j$ , making it crucial to execute the procedure efficiently to maintain computational feasibility. Hence, QT is particularly well-suited for studying systems where the Hamiltonian can be easily represented as a sparse matrix, as is the case, for example, in the Peierls model [10, 64] or even some systems with quadratic electron-phonon interactions [65].

#### ACKNOWLEDGMENTS

The author acknowledges useful discussions with Darko Tanasković and Veljko Janković, and also thanks Veljko Janković for sharing HEOM data from Refs. [36] and [37]. The author acknowledges funding provided by the Institute of Physics Belgrade through a grant from the Ministry of Science, Technological Development, and Innovation of the Republic of Serbia. A part of the numerical computations was performed on the PARADOX-IV supercomputing facility at the Scientific Computing Laboratory, National Center of Excellence for the Study of Complex Systems, Institute of Physics Belgrade.

- 
- [1] C. Jacoboni, *Theory of Electron Transport in Semiconductors: A Pathway from Elementary Physics to Nonequilibrium Green Functions* (Springer-Verlag Berlin Heidelberg, 2010).
- [2] J. M. Ziman, *Electrons and Phonons: The Theory of Transport Phenomena in Solids* (Oxford University

- Press, New York, 2001).
- [3] A. Troisi, Charge transport in high mobility molecular semiconductors: Classical models and new theories, *Chem. Soc. Rev.* **40**, 2347 (2011).
- [4] M. P. Marder, *Condensed matter physics* (John Wiley & Sons, 2010).



- [5] R. Kubo, Statistical-mechanical theory of irreversible processes. I. General theory and simple applications to magnetic and conduction problems, *J. Phys. Soc. Jpn.* **12**, 570 (1957).
- [6] G. Mahan, *Many-Particle Physics* (Kluwer Academic, New York, 2000).
- [7] B. Bertini, F. Heidrich-Meisner, C. Karrasch, T. Prosen, R. Steinigeweg, and M. Žnidarič, Finite-temperature transport in one-dimensional quantum lattice models, *Rev. Mod. Phys.* **93**, 025003 (2021).
- [8] S. Ciuchi, S. Fratini, and D. Mayou, Transient localization in crystalline organic semiconductors, *Phys. Rev. B* **83**, 081202 (2011).
- [9] S. Fratini, D. Mayou, and S. Ciuchi, The transient localization scenario for charge transport in crystalline organic materials, *Adv. Funct. Mater.* **26**, 2292 (2016).
- [10] A. Troisi and G. Orlandi, Charge-transport regime of crystalline organic semiconductors: Diffusion limited by thermal off-diagonal electronic disorder, *Phys. Rev. Lett.* **96**, 086601 (2006).
- [11] J. E. Runeson, T. J. G. Drayton, and D. E. Manolopoulos, Charge transport in organic semiconductors from the mapping approach to surface hopping, *J. Chem. Phys.* **161**, 144102 (2024).
- [12] N. Prodanović and N. Vukmirović, Charge carrier mobility in systems with local electron-phonon interaction, *Phys. Rev. B* **99**, 104304 (2019).
- [13] P. Mitrić, V. Janković, N. Vukmirović, and D. Tanasković, Spectral functions of the Holstein polaron: Exact and approximate solutions, *Phys. Rev. Lett.* **129**, 096401 (2022).
- [14] S. Fratini and S. Ciuchi, Dynamical mean-field theory of transport of small polarons, *Phys. Rev. Lett.* **91**, 256403 (2003).
- [15] S. Fratini and S. Ciuchi, Optical properties of small polarons from dynamical mean-field theory, *Phys. Rev. B* **74**, 075101 (2006).
- [16] P. Mitrić, V. Janković, N. Vukmirović, and D. Tanasković, Cumulant expansion in the Holstein model: Spectral functions and mobility, *Phys. Rev. B* **107**, 125165 (2023).
- [17] J.-J. Zhou and M. Bernardi, Predicting charge transport in the presence of polarons: The beyond-quasiparticle regime in SrTiO<sub>3</sub>, *Phys. Rev. Res.* **1**, 033138 (2019).
- [18] Y.-C. Cheng and R. J. Silbey, A unified theory for charge-carrier transport in organic crystals, *J. Chem. Phys.* **128**, 114713 (2008).
- [19] J. H. Fetherolf, D. Golež, and T. C. Berkelbach, A unification of the Holstein polaron and dynamic disorder pictures of charge transport in organic crystals, *Phys. Rev. X* **10**, 021062 (2020).
- [20] G. L. Goodvin, A. S. Mishchenko, and M. Berciu, Optical Conductivity of the Holstein polaron, *Phys. Rev. Lett.* **107**, 076403 (2011).
- [21] F. Ortmann, F. Bechstedt, and K. Haneewald, Theory of charge transport in organic crystals: Beyond Holstein's small-polaron model, *Phys. Rev. B* **79**, 235206 (2009).
- [22] L. Friedman, Electron-phonon interaction in organic molecular crystals, *Phys. Rev.* **140**, A1649 (1965).
- [23] S. H. Glarum, Electron mobilities in organic semiconductors, *J. Phys. Chem. Solids* **24**, 1577 (1963).
- [24] W. Li, J. Ren, and Z. Shuai, Finite-temperature TD-DMRG for the carrier mobility of organic semiconductors, *J. Phys. Chem. Lett.* **11**, 4930 (2020).
- [25] Y. Ge, W. Li, J. Ren, and Z. Shuai, Computational method for evaluating the thermoelectric power factor for organic materials modeled by the Holstein model: A time-dependent density matrix renormalization group formalism, *J. Chem. Theory Comput.* **18**, 6437 (2022).
- [26] D. Jansen, J. Bonča, and F. Heidrich-Meisner, Finite-temperature optical conductivity with density-matrix renormalization group methods for the Holstein polaron and bipolaron with dispersive phonons, *Phys. Rev. B* **106**, 155129 (2022).
- [27] J. Jaklič and P. Prelovšek, Lanczos method for the calculation of finite-temperature quantities in correlated systems, *Phys. Rev. B* **49**, 5065 (1994).
- [28] J. Jaklič and P. Prelovšek, Finite-temperature properties of doped antiferromagnets, *Adv. Phys.* **49**, 1 (2000).
- [29] P. Prelovšek and J. Bonča, Ground state and finite temperature Lanczos methods, in *Strongly Correlated Systems: Numerical Methods*, edited by A. Avella and F. Mancini (Springer Berlin Heidelberg, Berlin, Heidelberg, 2013) pp. 1–30.
- [30] H. Rammal, A. Ralko, S. Ciuchi, and S. Fratini, Transient localization from the interaction with quantum bosons, *Phys. Rev. Lett.* **132**, 266502 (2024).
- [31] G. Schubert, G. Wellein, A. Weisse, A. Alvermann, and H. Fehske, Optical absorption and activated transport in polaronic systems, *Phys. Rev. B* **72**, 104304 (2005).
- [32] A. Weiße, G. Wellein, A. Alvermann, and H. Fehske, The kernel polynomial method, *Rev. Mod. Phys.* **78**, 275 (2006).
- [33] S. Miladić and N. Vukmirović, Method for obtaining polaron mobility using real and imaginary time path-integral quantum Monte Carlo, *Phys. Rev. B* **107**, 184315 (2023).
- [34] A. S. Mishchenko, N. Nagaosa, G. De Filippis, A. de Candia, and V. Cataudella, Mobility of Holstein polaron at finite temperature: An unbiased approach, *Phys. Rev. Lett.* **114**, 146401 (2015).
- [35] Y.-C. Wang and Y. Zhao, Diagrammatic quantum Monte Carlo toward the calculation of transport properties in disordered semiconductors, *J. Chem. Phys.* **156**, 204116 (2022).
- [36] V. Janković, Holstein polaron transport from numerically “exact” real-time quantum dynamics simulations, *J. Chem. Phys.* **159**, 094113 (2023).
- [37] V. Janković, P. Mitrić, D. Tanasković, and N. Vukmirović, Vertex corrections to conductivity in the Holstein model: A numerical-analytical study, *Phys. Rev. B* **109**, 214312 (2024).
- [38] J. Vučičević, J. Kokalj, R. Žitko, N. Wentzell, D. Tanasković, and J. Mravlje, Conductivity in the square lattice Hubbard model at high temperatures: Importance of vertex corrections, *Phys. Rev. Lett.* **123**, 036601 (2019).
- [39] G. Cohen, E. Gull, D. R. Reichman, and A. J. Millis, Taming the dynamical sign problem in real-time evolution of quantum many-body problems, *Phys. Rev. Lett.* **115**, 266802 (2015).
- [40] A. Girard, A fast ‘Monte-Carlo cross-validation’ procedure for large least squares problems with noisy data,

- Numer. Math.* **56**, 1 (1989).
- [41] M. F. Hutchinson, A stochastic estimator of the trace of the influence matrix for Laplacian smoothing splines, *Commun. Stat. - Simul. Comput.* **18**, 1059 (1989).
- [42] A. K. Saibaba, A. Alexanderian, and I. C. Ipsen, Randomized matrix-free trace and log-determinant estimators, *Numer. Math.* **137**, 353 (2017).
- [43] A. Hams and H. De Raedt, Fast algorithm for finding the eigenvalue distribution of very large matrices, *Phys. Rev. E* **62**, 4365 (2000).
- [44] T. Iitaka and T. Ebisuzaki, Random phase vector for calculating the trace of a large matrix, *Phys. Rev. E* **69**, 057701 (2004).
- [45] R. A. Meyer, C. Musco, C. Musco, and D. P. Woodruff, Hutch++: Optimal stochastic trace estimation, in *Proceedings of the Symposium on Simplicity in Algorithms (SOSA)* (SIAM, Philadelphia, PA, 2021) pp. 142–155.
- [46] E. N. Epperly, J. A. Tropp, and R. J. Webber, Xtrace: Making the most of every sample in stochastic trace estimation, *SIAM Journal on Matrix Analysis and Applications* **45**, 1 (2024).
- [47] J. Schnack, J. Richter, and R. Steinigeweg, Accuracy of the finite-temperature Lanczos method compared to simple typicality-based estimates, *Phys. Rev. Res.* **2**, 013186 (2020).
- [48] T. Heitmann, J. Richter, D. Schubert, and R. Steinigeweg, Selected applications of typicality to real-time dynamics of quantum many-body systems, *Z. Naturforsch., A: Phys. Sci.* **75**, 421 (2020).
- [49] F. Jin, D. Willsch, M. Willsch, H. Lagemann, K. Michielsen, and H. De Raedt, Random state technology, *J. Phys. Soc. Jpn.* **90**, 012001 (2021).
- [50] C. Bartsch and J. Gemmer, Dynamical typicality of quantum expectation values, *Phys. Rev. Lett.* **102**, 110403 (2009).
- [51] P. Reimann, Dynamical typicality of isolated many-body quantum systems, *Phys. Rev. E* **97**, 062129 (2018).
- [52] R. Steinigeweg, J. Herbrych, F. Pollmann, and W. Brenig, Typicality approach to the optical conductivity in thermal and many-body localized phases, *Phys. Rev. B* **94**, 180401 (2016).
- [53] J. Richter and R. Steinigeweg, Combining dynamical quantum typicality and numerical linked cluster expansions, *Phys. Rev. B* **99**, 094419 (2019).
- [54] T. Monnai and A. Sugita, Typical pure states and nonequilibrium processes in quantum many-body systems, *J. Phys. Soc. Jpn.* **83**, 094001 (2014).
- [55] S. Sugiura and A. Shimizu, Thermal pure quantum states at finite temperature, *Phys. Rev. Lett.* **108**, 240401 (2012).
- [56] S. Sugiura and A. Shimizu, Canonical thermal pure quantum state, *Phys. Rev. Lett.* **111**, 010401 (2013).
- [57] T. A. Elsayed and B. V. Fine, Regression relation for pure quantum states and its implications for efficient computing, *Phys. Rev. Lett.* **110**, 070404 (2013).
- [58] R. Steinigeweg, J. Gemmer, and W. Brenig, Spin-current autocorrelations from single pure-state propagation, *Phys. Rev. Lett.* **112**, 120601 (2014).
- [59] T. Holstein, Studies of polaron motion: Part I. The molecular-crystal model, *Ann. Phys.* **8**, 325 (1959).
- [60] C. Franchini, M. Reticcioli, M. Setvin, and U. Diebold, Polarons in materials, *Nat. Rev. Mater.* **6**, 560 (2021).
- [61] V. Janković, Numerical study of the one-dimensional Holstein model using the momentum-space hierarchical equations of motion method (2023), Zenodo.
- [62] See Supplemental Material for additional numerical results and discussions.
- [63] P. Mitrić, V. Janković, V. Dobrosavljević, and D. Tanasković, Precursors to Anderson localization in the Holstein model: Quantum and quantum-classical solutions, arXiv:xxxx.xxxxx (2024).
- [64] S. Fratini and S. Ciuchi, Bandlike motion and mobility saturation in organic molecular semiconductors, *Phys. Rev. Lett.* **103**, 266601 (2009).
- [65] S. Ragni, T. Hahn, Z. Zhang, N. Prokof'ev, A. Kuklov, S. Klimin, M. Houtput, B. Svistunov, J. Tempere, N. Nagaosa, C. Franchini, and A. S. Mishchenko, Polaron with quadratic electron-phonon interaction, *Phys. Rev. B* **107**, L121109 (2023).

## Supplemental material for: Dynamical quantum typicality: A simple method for investigating transport properties applied to the Holstein model

Petar Mitrić,<sup>1</sup>

<sup>1</sup>*Institute of Physics Belgrade, University of Belgrade, Pregrevica 118, 11080 Belgrade, Serbia*

### A. CONVERGENCE OF THE CURRENT-CURRENT CORRELATION FUNCTION $C_{jj}(t)$ WITH RESPECT TO THE TOTAL NUMBER OF PHONONS $M$ IN THE HILBERT SPACE

In the main part of this paper, we examined the effectiveness of the (dynamical) quantum typicality (QT) method [S1, S2] in predicting transport properties, using the 1D Holstein model as an example. We presented the current-current correlation functions  $C_{jj}(t)$ , alongside related quantities such as optical conductivities  $\mu(\omega)$  and time-dependent diffusion constants  $D(t)$ , in a wide range of parameter regimes. Since the QT methodology is limited to finite-dimensional Hilbert spaces, we confined our study to systems with  $N$  lattice sites and restricted the total number of phonons to some finite value  $M$ . This quantity  $M$  had to be increased until the examined results no longer changed with further increases, ensuring convergence is achieved. This procedure had to be performed for each parameter regime separately. In this Section, we demonstrate how that looks like in practice. Before doing so, let us first address one theoretical question.

Within the QT method, why is it justified to truncate the total number of phonons to be less or equal to  $M$ , given that the Hilbert space is inherently infinite-dimensional? In other words, why can the wave function  $|\psi\rangle$ , used for stochastic trace estimation, be represented as a finite-dimensional column vector in the coordinate representation, even though QT requires  $|\psi\rangle$  to be constructed as a linear combination of an infinite number of basis vectors  $|i\rangle$ , with randomly chosen numbers  $c_i$  as coefficients  $|\psi\rangle = \sum_i c_i |i\rangle$ ; see Sec. II from the main text. The justification lies in the fact that the relevant quantity in Eqs. (8) and (9) of the main text is not  $|\psi\rangle$  directly, but rather  $|\psi_\beta\rangle = e^{-\beta H/2} |\psi\rangle$  and  $|\phi_\beta\rangle = j e^{-\beta H/2} |\psi\rangle$ . Therefore, we see that the contribution corresponding to basis vectors with large number of phonons is suppressed by the Boltzmann factor  $e^{-\beta H/2}$ .

Let us now return to the main question of how convergence with respect to  $M$  is achieved in practice. A straightforward procedure would consist of repeating the QT calculation for  $C_{jj}(t)$ , using progressively larger values of  $M$ , until convergence is reached. However, this is actually not necessary. As an alternative, we can go back to Eq. (9) from the main text, and analyze the scalar products in the numerator and denominator: in each of those scalar products, for each  $t$ , we can extract contributions corresponding to terms with total number of phonons less or equal to different values of  $M = 0, 1, 2, \dots$ . In such a way, repeating calculation for various  $M$  is not needed, since a single QT calculation is sufficient. Usually, we apply the described technique for somewhat smaller lattice  $N$ , estimate the necessary number of phonons per site  $M/N$ , and then conclude that the total number of phonons for any larger lattice then just needs to be scaled appropriately  $(M/N)N_{\text{larger}}$ .

In Figs. S1, S2 and S3, we show how this analysis looks like for the regimes corresponding to top panels in Figs. 1, 2 and 3 of the main text. For example, in Fig. S1 we see that the convergence of  $C_{jj}$  for all times  $t$  is achieved for  $M \approx 12$ . This calculation was performed on a lattice with  $N = 7$  sites. Hence, for the lattice with  $N = 11$  sites, which we analyzed in the main text, one should use  $M \approx 11 \cdot (12/7) \approx 18.86$ , which we round up to  $M = 20$ . This is why  $M = 20$  was used in the main text.

It is interesting to note that the required number of phonons for convergence, as shown in Figs. S1, S2, and S3, appears to be smaller for larger times  $t$ . This trend is observed across all regimes analyzed in the main text. This is likely a consequence of the fact that the states with a large number of phonons correspond to higher energies, causing their phase to change rapidly as a function of  $t$ , particularly at large times, after the time evolution operator  $e^{-iHt}$  is applied; see Eqs. (10) and (11) in the main text.

We note that while Figs. S1, S2, and S3 illustrate only the dependence of  $\text{Re } C_{jj}(t)$  on  $M$ , a similar analysis was also conducted independently for both the numerator and denominator of Eq. (9) from the main text. The reason why we do this, especially for the denominator, is because we want to make sure that the truncated Hilbert space can encompass all non negligible components of  $|\psi_\beta\rangle$ . This is important because the truncation of the Hilbert space can introduce error not only when calculating the scalar products (see Eq. (9) of the main text), but also when performing time evolution of wave functions (see Eqs. (10) and (11) in the main text).

Therefore, we introduced a convenient procedure for conducting convergence analysis with respect to  $M$ . Unfortunately, a similarly efficient approach for examining convergence with respect to  $N$  is not currently available. While

analyzing the optical sum rule can provide useful insights, the most reliable way to ensure that finite-size effects are absent is to simply apply QT to different lattice sites until convergence is achieved. An example of this analysis is given in Sec. B and showed in Fig. S5.

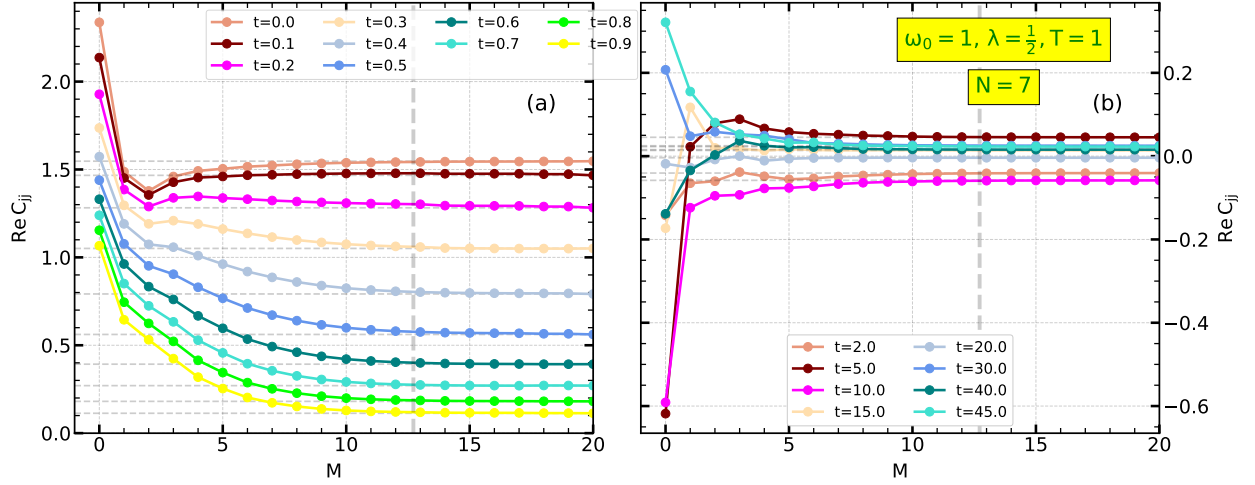


FIG. S1. Analyzing the convergence of the real part of the current current correlation function  $\text{Re } C_{jj}(t)$ , with respect to the number of phonons taken in the Hilbert space  $M$  for (a) small  $t$  (b) large  $t$ . The tick vertical dashed line represents our estimation of the number of phonons one should take for the results to be considered converged for all times  $t$ . The results are shown in the regime  $\omega_0 = 1$ ,  $\lambda = 1/2$ ,  $T = 1$  on a lattice with  $N = 7$  sites.

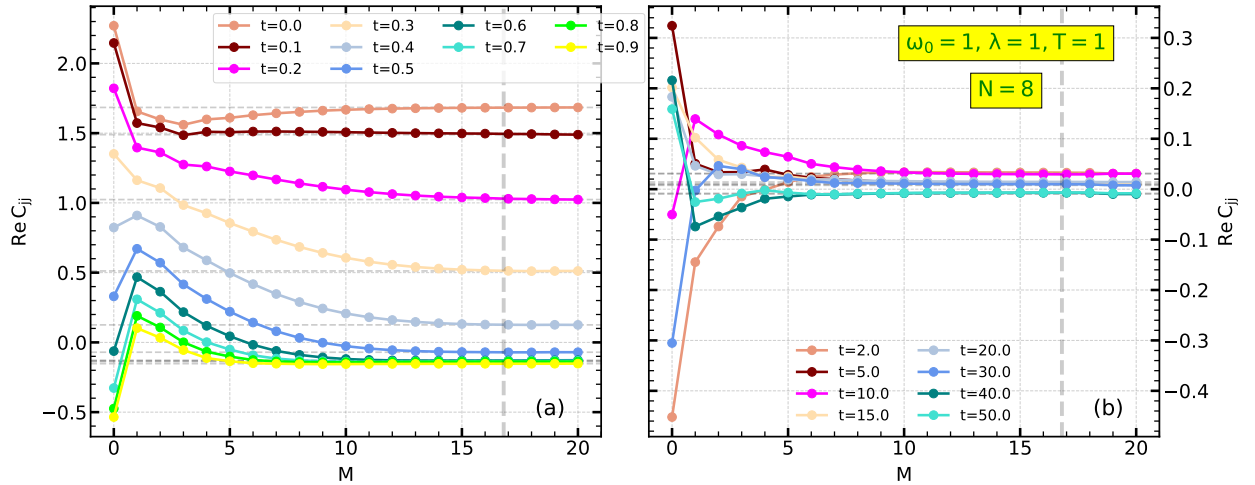


FIG. S2. Analyzing the convergence of the real part of the current current correlation function  $\text{Re } C_{jj}(t)$ , with respect to the number of phonons taken in the Hilbert space  $M$  for (a) small  $t$  (b) large  $t$ . The tick vertical dashed line represents our estimation of the number of phonons one should take for the results to be considered converged for all times  $t$ . The results are shown in the regime  $\omega_0 = 1$ ,  $\lambda = 1$ ,  $T = 1$  on a lattice with  $N = 8$  sites.

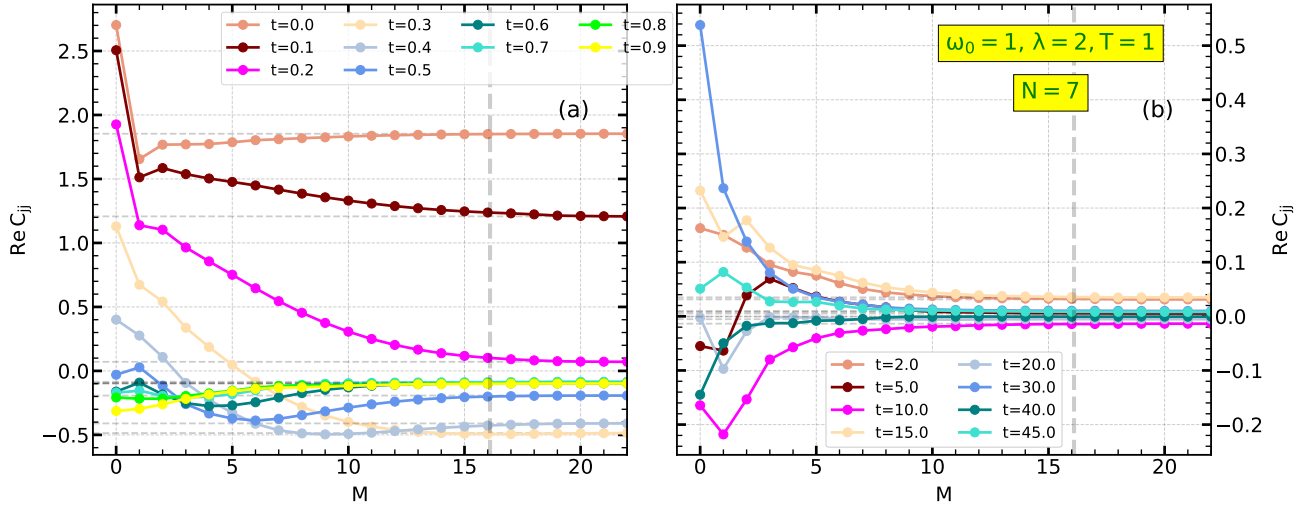


FIG. S3. Analyzing the convergence of the real part of the current current correlation function  $\text{Re} C_{jj}(t)$ , with respect to the number of phonons taken in the Hilbert space  $M$  for (a) small  $t$  (b) large  $t$ . The tick vertical dashed line represents our estimation of the number of phonons one should take for the results to be considered converged for all times  $t$ . The results are shown in the regime  $\omega_0 = 1$ ,  $\lambda = 2$ ,  $T = 1$  on a lattice with  $N = 7$  sites.

### B. A MORE DETAILED ANALYSIS OF THE REGIME $\omega_0 = \lambda = T = 1$

In the main text we analyzed the transport properties in the regime  $\omega_0 = \lambda = T = 1$ ; see Figs. 2(a<sub>1</sub>) and 2(a<sub>2</sub>) from the main text. We presented the QT results for two different lattice sizes, but the results using the hierarchical equations of motion (HEOM) [S3] benchmark were not available in this particular regime. At first glance,  $C_{jj}(t)$  and  $\mu(\omega)$  looked qualitatively as expected. However, the time dependent diffusion constant  $D(t)$  did not show any signs of saturation even after quite long propagation times. This suggests that further examination is required.

First of all, let us point out that Fig. S2 already explicitly demonstrated that  $\approx 2$  phonons per lattice site are enough to reach convergence with respect to the number of phonons. Therefore  $M = 20$  or more should be sufficient for lattices with  $N = 7, 8, 9, 10$  sites. This is always respected in Fig. S4, which illustrates that the absence of saturation of  $D(t)$  persists across different numerical settings, as we now discuss: first of all, for  $N = 7$  lattice sites with  $M = 30$  phonons, the time step in the Runge-Kutta propagation was set to  $dt = 0.01$ . We then reduced the time step 10 times, to  $dt = 0.001$ . As shown in Fig. S4, we see that neither of them leads to the saturation of  $D(t)$ . Hence, it is unlikely that this odd behavior of  $D(t)$  is a consequence of the insufficient number of phonons in the Hilbert space or the excessive Runge-Kutta time step. In addition to all of these, we also vary the lattice size, showing results for  $N = 7, 8, 9, 10$ . The peculiar large time behavior of  $D(t)$  is observed for all of them. Despite this, by inspecting how various cutoffs in time (for  $C_{jj}(t)$ ) influence the behavior of  $\mu(\omega)$ , we can conclude that  $\mu(\omega)$  is actually quite reliable for  $\omega \gtrsim |0.15|$ .

As a side note, let us also comment on the fact that although the two results for  $N = 7$  and  $M = 30$  look quite similar, some small differences in  $\mu(\omega)$  can be observed, and both of those results have some kind of noisy structure. This is a consequence of the fact that the effective dimension of the Hilbert space for  $N = 7$  (and even for  $N = 8$ ) is not that large, so approximating the traces, in Eq. (9) from the main text, by just a single random state is not actually extremely accurate. This is demonstrated in Fig. S5, where we plot QT results for  $N = 8$  using 10 different realizations of  $|\psi\rangle$ . The overall shape of  $\mu(\omega)$  can be discerned from individual random realizations, but accurate results are obtained only by using stochastic trace approximation (see Eq. (7) of the main text) with a few dozen different realizations of random state  $|\psi\rangle$ . In Fig. S5, the black line represents the averaged result that was actually the one we also used for Fig. S4. As a final remark, we note how these averaged results are obtained: different realizations of  $\text{Re} C_{jj}(t)$  are not averaged directly. Instead, numerators and denominators in Eq. (9) from the main text are averaged separately [S4], as explained by Eq. (7) from the main text. Quantities  $\mu(\omega)$  and  $D(t)$  are then simply obtained using Eqs. (3) and (4) from the main text.

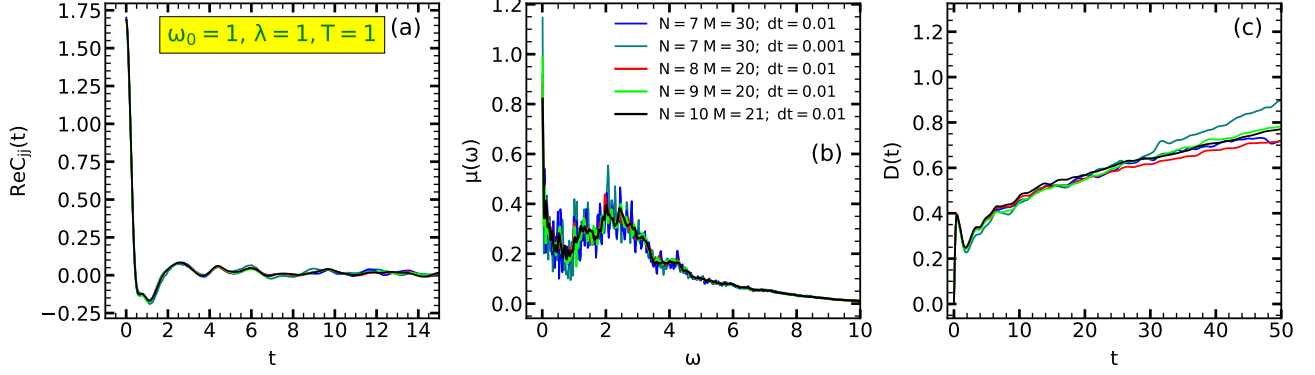


FIG. S4. Results for (a) the real part of the current-current correlation function  $\text{Re } C_{jj}(t)$  (b) frequency dependent mobility  $\mu(\omega)$  (c) time dependent diffusion constant  $D(t)$ , in the regime  $\omega_0 = \lambda = T = 1$  for different number of lattice sites  $N$ , total number of phonons  $M$ , and Runge-Kutta steps  $dt$ . We note that the results for  $N = 7, 9, 10$  were obtained using QT method, while  $N = 8$  result was obtained via stochastic trace approximation, with 30 random realizations. (QT is just a special case of the stochastic trace approximation with a single random realization. Larger number of realizations were used because the effective dimension of the Hilbert space is not very large; see the main text). We also emphasize that although  $N = 9$  and  $N = 10$  results are practically the same, the difference observed for  $\mu_{\text{DC}} = \mu(\omega = 0)$  is a consequence of the fact that  $N = 10$  results were propagated up to  $t \sim 60$ , while  $N = 9$  results were propagated up to  $t \sim 100$  (and  $D(t)$  kept increasing).

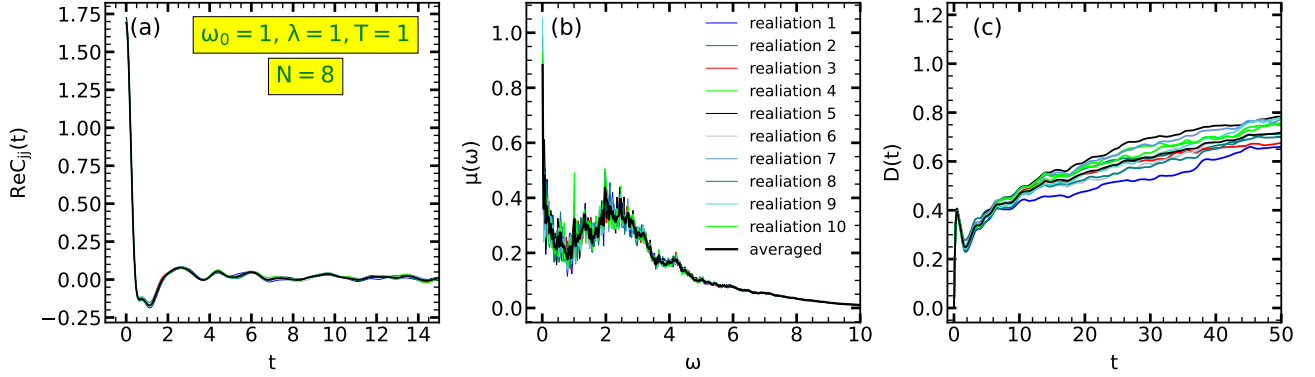


FIG. S5. Results for (a) the real part of the current-current correlation function  $\text{Re } C_{jj}(t)$  (b) frequency dependent mobility  $\mu(\omega)$  (c) time dependent diffusion constant  $D(t)$ , in the regime  $\omega_0 = \lambda = T = 1$  for  $N = 8$  lattice sites,  $M = 20$  phonons, and Runge-Kutta time step  $dt = 0.01$ . The non-black lines are QT results, obtained using different random vector  $|\psi\rangle$  realizations, while the black line is obtained using stochastic trace approximation with 30 random realizations. (QT is just a special case of the stochastic trace approximation with a single random realization. Larger number of realizations were used because the effective dimension of the Hilbert space is not very large; see the main text).

### C. ADDITIONAL RESULTS IN THE STRONG COUPLING REGIME $\lambda = 2$

In the main part of the text, in Fig. 3, we presented and analyzed the current-current correlation function  $C_{jj}(t)$ , the optical conductivity  $\mu(\omega)$ , and the time-dependent diffusion constant  $D(t)$  in the strong coupling regime  $\lambda = 2$  for  $\omega_0 = 1$  and  $T = 1, 10$ . For the sake of completeness, here we also show the results for  $T = 2$  and  $T = 5$ . As in the main text, convergence of the HEOM method with respect to the so-called maximum hierarchy depth could not be accomplished, which is why we show only QT and QMC results. QMC results are available only for  $T = 5$ , and they confirm that the accuracy of QT predictions of  $C_{jj}(t)$  are excellent for short times. At longer times, benchmarks for QT are unfortunately unavailable, although the saturation of diffusion  $D(t)$  and the presence of a bump in  $C_{jj}(t)$  at  $t = 2\pi/\omega_0$  indicate that QT should at least be qualitatively correct. Nevertheless, considering all the crosschecks performed so far, we expect these results to be also quantitatively accurate. As a final remark, let us point out that due to the large electron phonon coupling and high temperatures we do not expect the significant finite size effects

in the QT results, as suggested by the high accuracy with which the optical sum rule is satisfied. After all, this was explicitly demonstrated in the main text where we saw that  $N = 9$  was sufficient to reach thermodynamic limit at  $T = 1$ , while at  $T = 10$  the results practically already converged for  $N = 4$  sites.

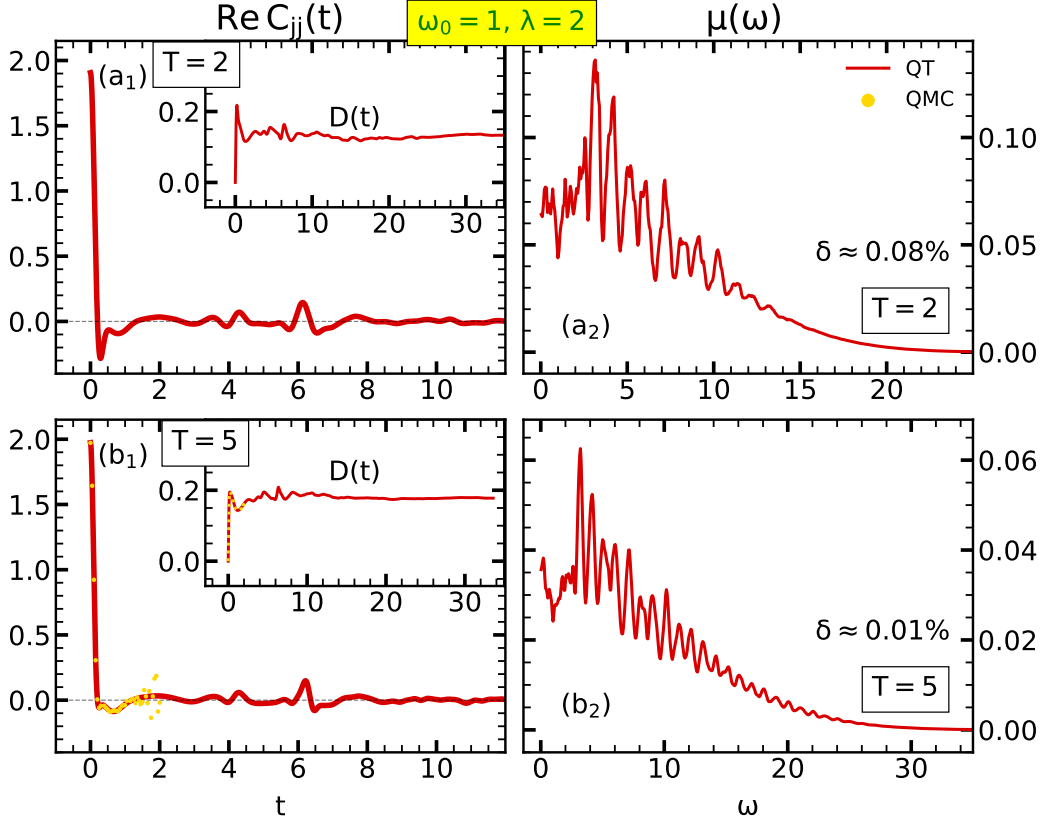


FIG. S6. Comparison of (a<sub>1</sub>)–(b<sub>1</sub>)  $C_{jj}(t)$  and (a<sub>2</sub>)–(b<sub>2</sub>)  $\mu(\omega)$  in the strong coupling regime  $\omega_0 = 1$ ,  $\lambda = 2$ , at  $T = 2, 5$ . The QMC results were reproduced from Fig. 8. of Ref. [S3]. Panels (a<sub>1</sub>)–(b<sub>1</sub>) also show the time dependent diffusion constant  $D(t)$  in the insets. The relative accuracy  $\delta$  with which the optical sum rule is satisfied within QT is shown in Panels (a<sub>2</sub>)–(b<sub>2</sub>). The total number of phonons and lattice sizes used are: (a<sub>1</sub>)–(a<sub>2</sub>)  $M^{\text{QT}} = 34$ ,  $N^{\text{QT}} = 7$ ; (b<sub>1</sub>)–(b<sub>2</sub>)  $M^{\text{QT}} = 70$ ,  $N^{\text{QT}} = 6$ , and  $N^{\text{QMC}} = 10$ . QMC results include statistical error bars

- 
- [S1] T. Heitmann, J. Richter, D. Schubert, and R. Steinigeweg, Selected applications of typicality to real-time dynamics of quantum many-body systems, *Z. Naturforsch., A: Phys. Sci.* **75**, 421 (2020).
- [S2] F. Jin, D. Willsch, M. Willsch, H. Lagemann, K. Michielsen, and H. De Raedt, Random state technology, *J. Phys. Soc. Jpn.* **90**, 012001 (2021).
- [S3] V. Janković, Holstein polaron transport from numerically “exact” real-time quantum dynamics simulations, *J. Chem. Phys.* **159**, 094113 (2023).
- [S4] J. Schnack, J. Richter, and R. Steinigeweg, Accuracy of the finite-temperature Lanczos method compared to simple typicality-based estimates, *Phys. Rev. Res.* **2**, 013186 (2020).